JOURNAL OF GEOPHYSICAL RESEARCH, VOL. 99, NO. D1, PAGES 1211–1223, JANUARY 20, 1994

Effect of vibrationally excited oxygen on ozone production in the stratosphere

K. O. Patten, Jr., P. S. Connell, D. E. Kinnison, and D. J. Wuebbles
Lawrence Livermore National Laboratory, Livermore, California

T. G. Slanger
SRI International, Menlo Park, California

L. Froidevaux
Jet Propulsion Laboratory, Pasadena, California

Photolysis of vibrationally excited oxygen produced by ultraviolet photolysis of ozone in the upper stratosphere is incorporated into the Lawrence Livermore National Laboratory two-dimensional zonally averaged chemical-radiative-transport model of the troposphere and stratosphere. The importance of this potential contributor of odd oxygen to the concentration of ozone is evaluated based on recent information on vibrational distributions of excited oxygen and on preliminary studies of energy transfer from the excited oxygen. When energy transfer rate constants similar to those of Toumi et al. [1991] are assumed, increases in model ozone concentrations of up to 4.0% in the upper stratosphere are found, and the model ozone concentrations are found to agree slightly better with measurements, including recent data from the Upper Atmosphere Research Satellite. However, the ozone increase is only 0.3% when the larger energy transfer rate constants indicated by recent experimental work are applied to the model. An ozone increase of 1% at 50 km requires energy transfer rate constants one-twentieth those of the preliminary observations. As a result, vibrationally excited oxygen processes probably do not contribute enough ozone to be significant in models of the upper stratosphere.

INTRODUCTION

Numerical simulations of stratospheric chemistry do not produce as large an ozone concentration as is found experimentally in the upper stratosphere [*World Meteorological Organization*, 1985; *Eluszkiewicz and Allen*, 1993]. This difference has been known for at least 15 years [*Butler*, 1978]. One of the possible explanations of this lower model-derived ozone concentration is that a source of odd oxygen is missing. *Slanger et al.* [1988] have proposed a possible additional source of odd oxygen based on experimental observation of dissociation of oxygen under photolysis at 248 nm. Photodissociation of ozone in the ultraviolet (200 to 310 nm) produces oxygen molecules in the ground electronic state:

$$O_3 + h\nu \rightarrow O_2\left({}^3\Sigma_g{}^-\right) + O\left({}^3P\right) \tag{1}$$

with a quantum yield of approximately 0.1 [*Valentini et al.*, 1987]. The molecular oxygen carries a large vibrational excitation [*Slanger et al.*, 1988; *Kinugawa et al.*, 1990]. The vibrationally excited oxygen $\left(O_2{}^\ddagger\right)$ then absorbs a second photon by its Schumann-Runge transition and dissociates:

$$O_2{}^\ddagger(\mathrm{v}) + h\nu \rightarrow 2O \tag{2}$$

This second dissociation can proceed with light considerably to the red of that required to dissociate thermal oxygen. In order to incorporate this mechanism into atmospheric models, the distribution of $O_2{}^\ddagger$ with respect to vibrational quantum number v and the rate constants for removal of Δ vibrational quanta from $O_2{}^\ddagger$ by collisional quenching;

$$O_2{}^\ddagger(v) + M \rightarrow O_2{}^\ddagger(v-\Delta) + M \tag{3}$$

must be known in detail.

Two previous studies have attempted to analyze the effects of $O_2{}^\ddagger$ chemistry on the stratosphere. *Toumi et al.* [1991] found an enhancement of ozone concentration ranging from 13% to 60% for altimtudes of 36 to 58 km in their atmospheric model using $O_2{}^\ddagger$ distributions from *Kinugawa et al.* [1990] and v–v quenching rate constants for $O_2{}^\ddagger$ based on *Rapp* [1965]. A later study by *Toumi* [1992] incorporating more thorough modeling of collisional quenching found that the ozone enhancement ranged from 1% to 4% in the 36- to 58-km altitude range, depending on the choice of fit to the *Kinugawa et al.* [1990] data.

The O_3 photolysis data of *H. Park and T.G. Slanger* [1994] indicate an $O_2{}^\ddagger(v)$ distribution different from *Kinugawa et al.* [1990], and preliminary collisional quenching data in a related study indicate a considerably higher rate constant than is suggested by the standard models and previous data. The photolysis and quenching of $O_2{}^\ddagger$ have been incorporated into the Lawrence Livermore National Laboratory (LLNL) global

Paper number 93JD02549
0148-0227/94/93JD-02549$05.00

two-dimensional chemical-radiative-transport model. This study compares the ozone concentrations calculated using both the previous collisional quenching parameters and the new experimental quenching data with observed ozone concentrations, including recent measurements from the Upper Atmosphere Research Satellite Microwave Limb Sounder (UARS MLS). An initial report of this work was presented at the International Quadrennial Ozone Symposium by *Patten et al.*

MODEL DESCRIPTION

The standard LLNL zonally averaged two-dimensional chemical-radiative-transport model of the Earth's atmosphere has been discussed previously [*Johnston et al.*, 1989; *Wuebbles et al.*, 1991]. The current version of the LLNL zonally averaged two-dimensional chemical-radiative-transport model determines the atmospheric distributions of 47 chemically active atmospheric trace constituents in the troposphere and stratosphere. The model domain extends from pole to pole in latitude, and from the ground to 60 km in altitude. The sine of latitude is used as the horizontal coordinate, with uneven increments corresponding to approximately 10°. The vertical coordinate corresponds to the natural logarithm of pressure; the scale height is 7.2 km and surface pressure is 1013 mb. The vertical resolution is 1.5 km in the troposphere and 3 km in the stratosphere.

Transport. In the dynamics portion of the two dimensional code, the circulation field is derived internally, in a similar manner to *Garcia and Solomon* [1983]. In our model, we use climatological temperature and zonal mean wind fields; both the temperature and zonal mean wind field vary continuously over the annual cycle. The temperature field is based on the reference model of *Barnett and Corney* [1985], while the zonal mean wind is based on data of *Fleming et al.* [1988]. The method used to obtain the circulation combines the zonal mean momentum equation and the thermodynamic equation into a form that, along with the thermal wind equation, yields a second-order diagnostic equation for the residual mean meridional stream function. This stream function is defined so that the continuity equation is solved exactly. The coefficients of the stream function terms on the left side of the equation are functions of known quantities. The right-hand side of the stream function equation includes the net heating rate term and the Eliassen-Palm flux representing wave driving. The net heating rate is calculated knowing the temperature and chemical species distribution and includes latent heating. The present code calculates the Eliassen-Palm flux directly from the zonal mean momentum equation. The right-hand side also includes a very small value of Rayleigh friction (value of about 0.1 day^{-1}) to account for small-scale disturbances. With all terms known, the second-order equation for the stream function is evaluated from which the velocity fields are then obtaineds.

The transport of chemical species is accomplished through both advection and turbulent eddy transport. Advection terms are treated using the second-order, two-dimensional transport algorithm of *Smolarkiewicz* [1984]. The transport caused by eddy motion is parameterized through the diffusion coefficients K_{yy} and K_{zz}. Values of K_{zz} do not vary with annual cycle, but are different within the troposphere and stratosphere. The value of K_{zz} in the troposphere is 4 m^2/s, while K_{zz} in the stratosphere has a value of 0.1 m^2/s. Values of K_{yy} in the stratosphere are calculated using a method similar to that of *Newman et al.* [1988] by dividing the zonal mean momentum equation (i.e., the Eliassen-Palm flux) by the horizontal gradient of the quasi-geostrophic potential vorticity. In the stratosphere, a minimum value of K_{yy} has been established as $1\times10^5\ \mathrm{m}^2/\mathrm{s}$. The values of K_{yy} in the troposphere for the current model are assigned a value of $1\times10^6\ \mathrm{m}^2/\mathrm{s}$. The tropopause is treated as an annual mean, but latitude-dependent, function of the temperature field. The height of the tropopause varies from 8 km near the poles to 14 km at the equator.

Radiative transfer. To capture the spectral detail needed for photodissociation calculations, our two-stream multiple-layer UV-visible model uses 126 wavelength bins between 175 nm and 735 nm. In this approach, solar radiation is divided into direct solar radiation, downward diffuse radiation, and upward diffuse radiation. The scattering of energy from the direct solar beam within each individual layer is treated using the delta-Eddington algorithm, which includes the dependence of scattering and absorption on the solar zenith angle. The scattering of diffuse radiation (i.e., previously scattered radiation) from each individual layer is modeled using the simpler Sagan-Pollack algorithm. Both algorithms allow inclusion of the bulk optical properties of clouds and aerosols. Finally, the adding method is used to calculate irradiances throughout the vertically inhomogeneous atmosphere.

The RADIR infrared model that we have been using for several years is a version of the model described by *Harshvardhan et al.* [1987]. For our usage, it has been modified to improve the accuracy in the upper stratosphere. It includes absorption and emission by CO_2, O_3, and H_2O. It is based on wideband parameterizations fit to line-by-line calculations. Inhomogeneous absorption paths are included by pressure- and temperature-weighted scaling of trace gas absorber amounts. The model provides for specification of fractional cloud cover within each vertical model layer. Separate fractions can be specified for convective (deep, overlapping) and randomly overlapped clouds.

Chemistry. The photochemistry in the LLNL two-dimensional model represents the tropospheric and stratospheric interactions of actinic solar flux with the individual species in the families O_x, NO_y, ClO_y, HO_y, BrO_y, and CH_4 and its oxidation products. This part of the mechanism incorporates 43 transported species and four species for which abundance is determined through the assumption of instantaneous equilibrium. Source gases used include NO_x, N_2O, CH_4, CO_2, CO, the chlorine compounds CFC-11, CFC-12, CFC-113, CFC-114, CFC-115, HCFC-22, CCl_4, CH_3CCl_3, CH_3Cl, and the bromine compounds CH_3Br, CF_2ClBr, and CF_3Br. These gases are set to constant concentration at the ground except for a constant flux of NO_x. Most of the rates for the 111 thermal reactions in the model were taken from the NASA Panel recommendations [*DeMore et al.*, 1990]. However, the recent rate constant of *Vaghjiani and Ravishankara* [1991] is used for the reaction CH_4 + OH. The level of water vapor is assigned its climatological value, following the specific humidity of the *Oort* [1983] climatology, everywhere below the hydropause. Above the hydropause, water vapor is treated as a transported species; methane oxidation is its major source in this region of the atmosphere.

Forty-eight photolysis reactions occur in the LLNL model. The photolytic loss rate constants are calculated by integrating the product of absorption coefficient, quantum yield, and solar flux over wavelength (i.e. from 175 nm to 760 nm). The exoatmospheric solar flux is from *WMO* [1985]. The solar flux is then calculated as a function of altitude, latitude, and season at each time step, including the effects of absorption by O_2 and O_3 and multiple molecular (Rayleigh) scattering. The absorption cross sections and quantum yields include temperature and pressure dependence where appropriate and available. The Schumann-Runge band region of the O_2 absorption is treated using the technique of *Allen and Frederick* [1982], modified to match the more recent lower cross sections of the O_2 Herzberg continuum region. The photolysis of NO is also treated through the parameterization technique of *Allen and Frederick* [1982].

Members of the ClO_y family currently thought to play a role in the Antarctic spring, such as the ClO dimer, are included, but polar stratospheric aerosol surface is not included in this study. A representation of background stratospheric sulfuric acid aerosol surface is incorporated into the model, following the recommendations from the *WMO*, [1991] report. The reactions of N_2O_5 and $ClONO_2$ with H_2O on the aerosol surface are parameterized as first-order loss processes with rate constants determined by specified surface area density, collision frequency, and reaction probability.

The nonlinearity of the photochemistry with respect to diurnal averaging is accounted for through the calculation of individual altitude, latitude, and seasonally varying factors for each photochemical process. Full diurnal variability of each species is calculated beforehand for four seasons. The factors, relating individual process rates from the full diurnal calculation to the diurnally averaged values, are then spline interpolated for each time step.

EXCITED OXYGEN CHEMISTRY

In addition to the standard model, the rate of photolysis of O_3 into the ground state oxygen channel $\left(O_2\left({}^3\Sigma_g^-\right)\right)$ for each radiation bin is supplied to a model of $O_2^\ddagger$ processes. As is detailed below, the $O_2^\ddagger$ model internally performs three steps for each altitude-latitude combination. The nascent distribution of $O_2^\ddagger(v)$ is first found from O_3 photolysis rates. Rate constants for $O_2^\ddagger$ photolysis are calculated from the absorption cross sections. Finally, with the photolysis and energy transfer rate constants, the steady state concentration of $O_2^\ddagger(v)$ and the rate of photolysis of $O_2^\ddagger(v)$ are determined.

When O_3 is photolyzed with light of wavelength λ nm, or energy $E_\lambda = \left(10^7/\lambda\right)\text{cm}^{-1}$, the energy is distributed among that required to break an O-O bond D_0, that of translation (between the centers of mass of O_2 and O atom) E_T, that of rotation of the O_2 fragment E_r, and that of O_2 vibration E_v. The distribution of O_2 vibrational states v produced by photolysis at energy E_λ determines the rate of formation of $O_2^\ddagger$. Thus, a fit to the available experimental data on vibrational distributions on $O_2^\ddagger$ from O_3 photolysis in the wavelength range 200–320 nm is required. Data are available at two photolysis wavelengths in this range. *Park and Slanger* [1994] obtain a bimodal distribution of vibrational states in product O_2 when photolyzing O_3 at 248 nm. A study by *Kinugawa et al.* [1990] of O_3 photolyzed at 226 nm in a molecular beam shows two peaks of O atom with respect to translational energy. The peak at lower translational energy (higher O_2 vibrational quantum number) is reported as partially but not completely due to thermal decomposition of O_3. *Toumi* [1992] used the final state interaction (FSI) photolysis model, which produces a Poisson-like $O_2^\ddagger(v)$ distribution determined by the average vibrational quantum number produced, $\langle v \rangle$, and by the maximum possible vibrational quantum number given the photolysis energy, v_{max}. The FSI model cannot represent the bimodal distribution found by *Park and Slanger* [1994]. We therefore develop below a bimodal empirical fit to O_3 data at both photolysis wavelengths and extend this model for photolysis wavelengths from 200 to 320 nm, for which $O_2^\ddagger$ production is important.

The $O_2^\ddagger(v)$ data of Park and Slanger are first converted into terms of translational energy E_T for comparison. The vibrational energy E_v for each vibrational state v observed is calculated from the six-term power series of *Laher and Gilmore* [1991], $E_v = w_e(v+\frac{1}{2}) - w_e x_e(v+\frac{1}{2})^2 + w_e y_e(v+\frac{1}{2})^3 + w_e z_e (v+\frac{1}{2})^4 + \omega_e a_e(v+\frac{1}{2})^5 + \omega_e b_e(v+\frac{1}{2})^6$. The translational energy E_T corresponding to the v state is then known from the photolysis energy, the ozone dissociation energy, and the vibrational energy if the rotational energy is ignored. When data from both photolysis wavelengths are superimposed in terms of E_T, the higher E_T (lower v) peak does not vary significantly in average energy or energy width. The lower E_T (higher v) peak of *Kinugawa et al.* is uncertain due to possible thermal decomposition, so that we choose a double-Gaussian fit based upon all Park and Slanger observations and the higher E_T peak of *Kinugawa* et al.:

$$f(E_T) = N\left[0.3\ \exp\left(\frac{-(E_T - 0.5)^2}{2(0.3)^2}\right) + \exp\left(\frac{-(E_T - 2.5)^2}{2(0.5)^2}\right)\right] \quad (4)$$

where E_T is given in $eV\left(1\,eV = 8065\text{cm}^{-1}\right)$ with the condition that E_T is never less than zero, N is a normalization constant such that the integral of $f(E_T)$ from $E_T = 0$ to the photolysis energy is unity, and the means and spreads of the Gaussians and the multiplier 0.3 for the lower-E_T Gaussian are empirically fitted to the observations. The vibrational distribution is calculated using the E_v expression given above.

Figure 1*a* compares the Park and Slanger data (squares) at 248 nm with our fit (diamonds) and the fit of *Toumi* [1992] for both the $\langle v \rangle = v_{max}/2$ (Toumi case A) and $\langle v \rangle = v_{max}/2 + 2$ (Toumi case B) fits. Toumi case B tends toward more $O_2^\ddagger$ at higher v than does Toumi case A. Our fit and the FSI model are compared with the 226 nm data of *Kinugawa et al.* [1990] in Figure 1*b*. In Table 1, root-mean-square deviations between the observations and our fits and those of the FSI formula are compared. Our fit represents the Park and Slanger data somewhat better than the FSI model for 248-nm photolysis, but the *Toumi* [1992] case A represents the 226-nm photolysis somewhat better than does our fit. Figure 1*c* shows vibrational distributions calculated using equation (4) for four of the central energies of the LLNL model radiation bins.

The empirical double-Gaussian fit used in this study can best be regarded as preliminary due to the relatively limited coverage of the range of photolysis wavelengths of concern and to the uncertainty in the newly observed higher v peak in the $O_2^\ddagger$ distribution. *Toumi* [1992] has pointed out previously that further experimental work on the oxygen vibrational distribution from ozone photolysis is needed, and distributions at other photolysis wavelengths would contribute greatly to the current problem. Further, more recent analysis of the *Park and Slanger* [1994] data indicates that the double-Gaussian fit may overestimate the high-v second peak. We also find that more experimental study of $O_2^\ddagger(v)$ distributions from O_3

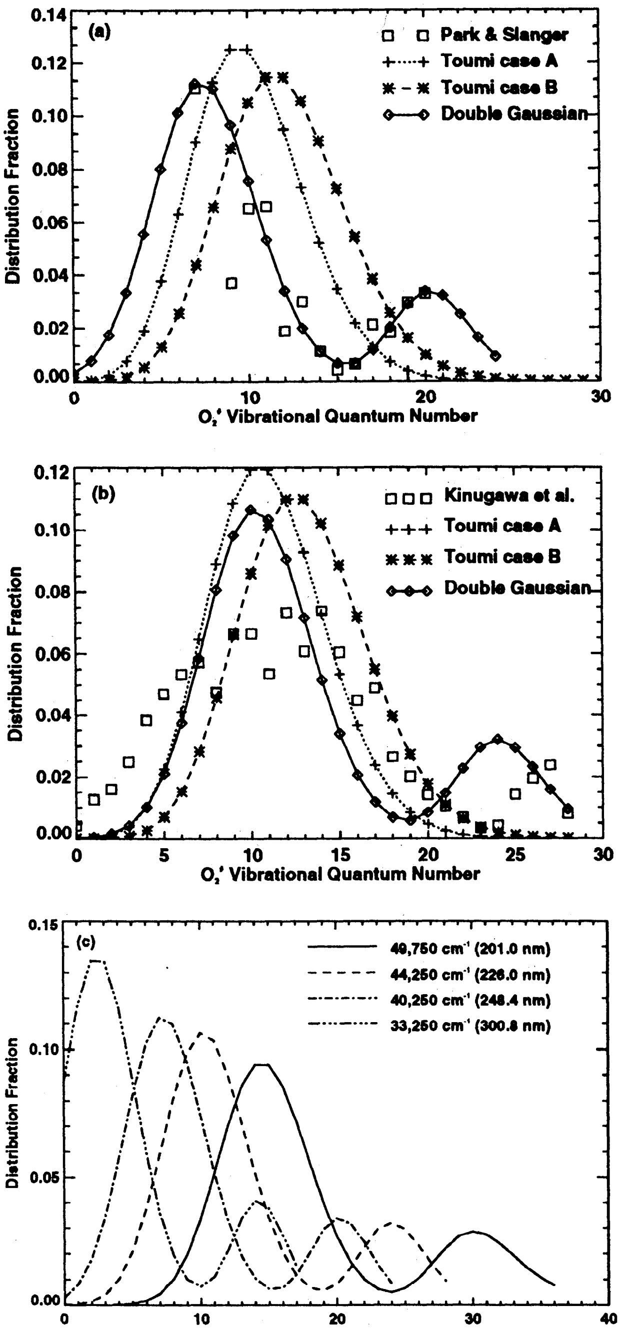

Fig. 1. Fit to nascent vibrationally excited oxygen ($O_2^\ddagger$) distribution from ozone photolysis at selected energies for the LLNL two-dimensional model (*a*) compared with 248 nm data of *Park and Slanger* [1994]; (*b*) compared with 226-nm data of *Kinugawa et al.* [1990]; and (*c*) at photolysis energies 49,750 cm^{-1}, 44,250 cm^{-1}, 40,250 cm^{-1}, and 33,250 cm^{-1} corresponding to four radiative energy bins of the LLNL two-dimensional model.

TABLE 1. Root-Mean-Square Deviations Between Oxygen Vibrational Distribution Fits and Data For Ozone Photolysis

H. Park and T.G. Slanger [1994], λ = 248 nm	
Current	0.0597
Toumi [1992],	
$<v> = \nu_{max}/2$	0.0796
$<i> = \nu_{max}/2 + 2$	0.0749

Kinugawa *et al.* [1990], λ = 226 nm	
Current	0.0227
Toumi [1992]	
$<v> = \nu_{max}/2$	0.0155
$<i> = \nu_{max}/2 + 2$	0.0272

photolysis in the 200- to 320-nm range are necessary, particularly with respect to characterizing the second, higher v peak.

Absorption cross sections for $O_2^\ddagger$ in the Schumann-Runge region are also required in the vibrationally excited oxygen photolysis rate constant calculation. However, experimental absorption cross sections for this species are not currently available in the known literature. Sufficiently accurate cross sections can instead be derived from quantum mechanical calculations based on those in *Levine* [1975] and *Saxon and Slanger* [1991]. First, the vibrational wave functions of the ground and excited states are required. The method of *Truhlar* [1972] as implemented by *Kulander* [1988] provides these wavefunctions for diatomic molecules given the vibrational potential surface. Vibrational potential surfaces of ground O_2 $\left({}^3\Sigma_g^-\right)$ and excited O_2 $\left({}^3\Sigma_u^-\right)$ [*Krupenie*, 1972] are extrapolated using r^{-12} dependence (r < 1.34 Å) to r = 0.506 Å and exp ($-\alpha r$) (r > 2.58 Å) to r = 5.67 Å for the overlap calculation below. Second, the oscillator linestrength $f_{v',v''}$ for the Schumann-Runge transition from vibrational state v'' in the ground electronic state to vibration v' in the excited electronic state is determined using the equation:

$$f_{v',v''} = \left(\frac{8\pi^2 m_e c}{3he^2}\right)\nu_{v',v''}\left|\langle v'|D(r)|v''\rangle\right|^2 \tag{5}$$

In this equation, the term $|< v'|D(r)|v''>|^2$ is Dirac "bra-ket" notation. The $<v'|$ represents the upper electronic state vibrational wave function, $D(r)$ is the Schumann-Runge transition dipole moment operator [*Allison et al.*, 1986], and $|v''>$ is the ground electronic state vibrational wave function. The product of these three terms is integrated over O-O radius r, then squared to give $|< v'|D(r)|v''>|^2$. The transition frequency between the two states $\nu_{v',v''}$ is found from the vibrational power series expansions for the ground [*Laher and Gilmore*, 1991] and excited [*Creek and Nicholls*, 1975; *Cheung et al.*, 1986; *Lewis et al.*, 1986] electronic states. The m_e is the electron mass, c is the speed of light in a vacuum, h is Planck's constant, and e is the fundamental charge. Finally, the $O_2^\ddagger$ absorption cross sections are calculated from the oscillator strength using the equation

$$\sigma_{v',v''} = \frac{\pi e^2}{m_e c^2} f_{v',v''}\rho(v') \tag{6}$$

where $\rho(v')$, the density of vibrational states in the excited electronic state, is taken as the first derivative of the excited electronic state E_v power series with respect to v. The transition oscillator strengths produced agree to within 50% with the experimentally established oscillator strengths of *Lewis et al.* [1986] and calculated oscillator strengths of *Allison et al.* [1971]. Absorption cross sections agree reasonably with the $v = 12$ cross sections used by *Saxon and Slanger* [1991]. Our cross sections are plotted for several v in Figure 2.

The removal of vibrational excitation from $O_2^{\ddagger}$ (equation (3) above) involves multiple processes. The $O_2^{\ddagger}$ vibration may lose excitation by two mechanisms of collisional transfer. $O_2^{\ddagger}$ vibrational energy may be transferred to translational and rotational energy in the collider; these two mechanisms are combined and designated as vibrational-to-translational, or *v-t*, transfer below. $O_2^{\ddagger}$ vibrational energy may also become vibrational energy in a collider molecule, which is designated as vibrational-to-vibrational, or *v-v*, transfer below. Either transfer mechanism preferentially removes one quantum of vibrational energy from $O_2^{\ddagger}$. Unlike the case for *v-t* transfer, the rate constants for *v-v* removal of two or more quanta of vibrational energy from $O_2^{\ddagger}$ remain significant [*Yardley*, 1980]. *Toumi et al.* [1991] incorporated only O_2 removal of one quantum from $O_2^{\ddagger}$ by *v-v* quenching. The later study of *Toumi* [1992] accounted for *v-v* quenching by O_2, which allowed removal of more than one quantum from $O_2^{\ddagger}$ and also included v-t quenching by N_2, O_2, and O atoms. Preliminary studies of $O_2^{\ddagger}$ (v = 8, 14, 18-22) quenching at SRI International indicate markedly larger rate constants than were used by *Toumi* [1992]. We will discuss the pertinent rate constants and our $O_2^{\ddagger}$ quenching rate constant fit below.

Nitrogen and oxygen as colliders have approximately the same energy transfer rate constant at $v = 22$ of $3.0\times10^{-15}\,\mathrm{cm}^3\,\mathrm{molecule}^{-1}\mathrm{s}^{-1}$. Quenching rate constants in *v-v* transfer depend mostly on the vibrational fundamental frequency of the collider gas, which is considerably different between N_2 and O_2. Thus, the *v-t* transfer process should dominate for that v level. *Yardley* [1980] has illustrated a proof that the probability of *v-t* energy transfer (and the rate constant) is directly proportional to the quantum number of the vibrationally excited species. Dividing the observed N_2 and O_2 rate constant of 3.0×10^{-15} by $v = 22$ gives a proportionality constant of $1.36\times10^{-16}\,\mathrm{cm}^3\mathrm{molecule}^{-1}\mathrm{s}^{-1}$ per vibrational quantum level in $O_2^{\ddagger}$ for all temperatures and for both N_2 and O_2 colliders. This *v-t* quenching rate constant is markedly larger than that of *Toumi* [1992], $k_{v-t} = 6.8\times10^{-19}$ $v\,\mathrm{cm}^3\mathrm{molecules}^{-1}\mathrm{s}^{-1}$, at all quantum numbers v.

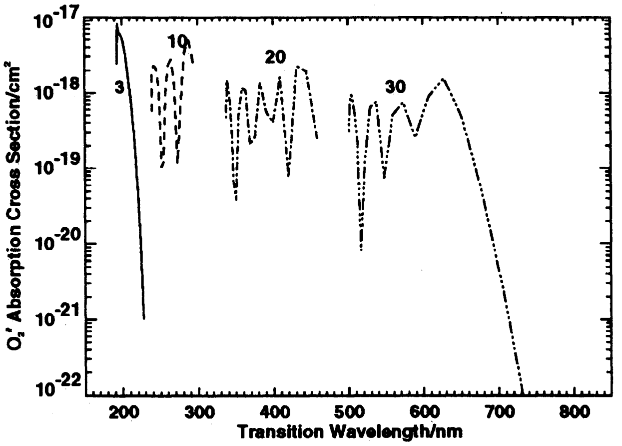

Fig. 2. Absorption cross sections for $O_2^{\ddagger}$ in several vibrational states are compared. These cross sections are calculated from vibrational wave functions obtained using the code of *Kulander* [1988] and *Truhlar* [1972].

The preliminary observations on collisions with N_2 for $O_2^{\ddagger}$(18-22) also indicate that v-v transfer removing two quanta of vibrational energy from $O_2^{\ddagger}$ is significant. A model proposed by *Rapp and Englander-Golden* [1964] and by *Rapp* [1965], as further expanded to multiple-quantum removal by *Yardley* [1980], provides the *v-v* energy transfer probability (fraction of collisions that results in *v-v* transfer) used in this study. *Rapp and Englander-Golden* [1964 equation (19)] provided the probability of a single quantum loss $P_{v,v+1}$ is

$$P_{v,v+1} = \sin^2\left(\frac{\pi\mu v_0 V'_{rs,pq}}{4\hbar k}\right)\mathrm{sech}^2\left(\frac{\pi\gamma}{4kv_0}\right), \tag{7}$$

for which k is Boltzmann's constant and $\hbar$ is Planck's constant divided by 2π. The $V_{rs,pq}{}'$ term is an interaction term integrated over the harmonic oscillator wave functions of the initial state of $O_2^{\ddagger}$, Ψ_p, the collider molecule initial wave function Ψ_p, and the final wave functions of the two molecules Ψ_r and Ψ_s:

$$\begin{aligned} V'_{rs,pq} &= \int_{-\infty}^{\infty} \Psi_r^{O_2^{\ddagger}}(Y_1)\exp\left\{\frac{m_O}{m_O+m_O}\frac{Y_1}{L}\right\}\Psi_p^{O_2^{\ddagger}}(Y_1)\,dY_1\cdot \\ &\quad \int_{-\infty}^{\infty}\Psi_s^{CD}(Y_2)\exp\left\{\frac{m_D}{m_C+m_D}\frac{Y_2}{L}\right\}\Psi_q^{CD}(Y_2)\,dY_2 \\ &= \exp\left(\alpha_{O_2}^2\right)\exp\left(\alpha_{CD}^2\right)\left(\frac{2^{p-r+1}r!}{p!}\right)^{\frac{1}{2}}\alpha_{O_2}^{p-r}\cdot \\ &\quad \alpha_{CD}L_r^{p-r}\left(-2\alpha_{O_2}^2\right)L_1^1\left(-2\alpha_{CD}^2\right) \end{aligned} \tag{8}$$

based on the evaluation of these integrals in *Rapp and Sharp* [1963]. For the above, $\alpha_Z = \left(4L\beta_Z{}^{1/2}\right)^{-1}$, where Z is either O_2 or N_2 and $\beta = 2\pi\mu\nu/h$. The generalized Laguerre polynomials $L_a{}^b(x)$ are calculated using Mathematica™ [*Wolfram*, 1988] for the values of α needed. The relative-velocity dependent probability calculated in this way is then integrated over the Maxwell distribution function in order to produce the probability of *v-v* energy transfer per collision [*Yardley*, 1980]:

$$\begin{aligned} \left\langle\left\langle P_{r\leftarrow p}\right\rangle\right\rangle &= \int_0^{\infty}\frac{gP_{r\leftarrow p}(g)}{\langle g\rangle}f(g)\,dg \\ &= 2\left(\frac{\mu}{2kT}\right)^2\int_0^{\infty}g^3\exp\left(-\frac{\mu}{2kT}g^2\right)\cdot \\ &\quad \left[\sin^2\left(c_1V'_{r\leftarrow p}g\right)\mathrm{sech}^2\left(\frac{c_2\lambda}{g}\right)\right]dg \end{aligned} \tag{9}$$

where $c_1 = 2\mu L/\hbar c_2 = 4\pi cL$, and λ is the difference in energy between final and initial states in cm^{-1} given $c = 2.998\times10^{10}\,\mathrm{cm\,s}^{-1}$. In accord with *Rapp and Englander-Golden* [1964], we estimate the integral from the value of the integrand at g which maximizes $g^3\exp\left(-\mu g^2/2kT\right)$, so that

$$\left\langle\left\langle P_{r\leftarrow p}\right\rangle\right\rangle = \frac{12\mu L^2k}{\hbar^2}\left(V'_{r\leftarrow p}\right)^2 T\,\mathrm{sech}^2\left(4\pi cL\left(\frac{\mu}{3kT}\right)^{\frac{1}{2}}\lambda\right) \tag{10}$$

Using the interaction characteristic length $L = 2.0\times10^{-11}$ m,

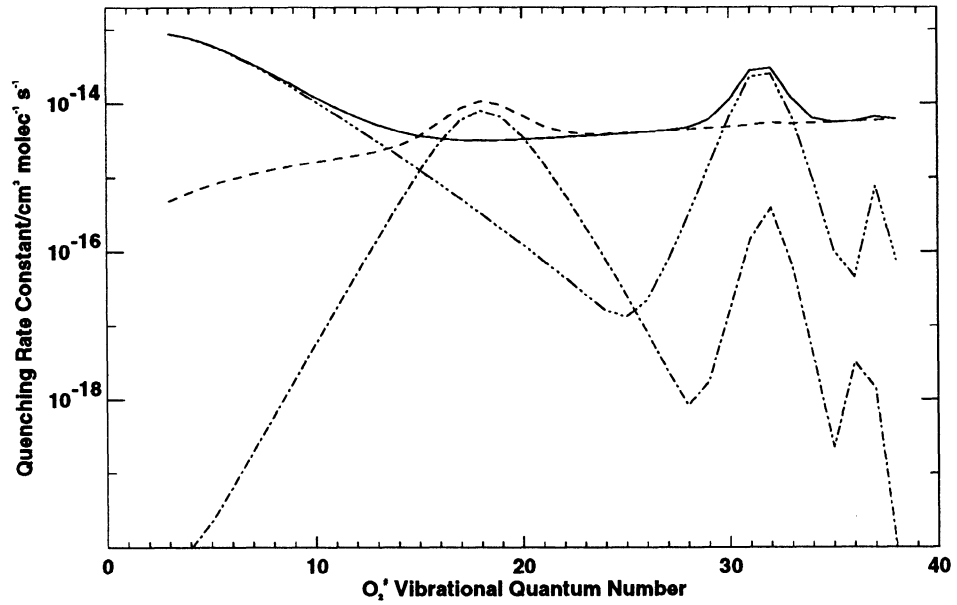

Fig.3. Collisional energy transfer rate constants for nitrogen (N_2) and oxygen (O_2) in accord with data obtained by Slanger and vibrational-to-vibrational energy transfer modeled by the *Yardley* [1980] extensions to *Rapp* [1965] are demonstrated for a temperature of 300 K. Three-dot-dashed line, O_2 *v-v* only; solid line ,O_2 *v-v* and *v-t*: one-dot-dashed line, N_2 *v-v* only; dashed line, N_2 *v-v* and *v-t*.

cited as typical by *Yardley* [1980], provides the *v-v* transfer probability used in the $O_2^\ddagger$ model. The rate constant for *v-v* energy transfer is that probability times the hard-sphere collision rate constant. Equation (10) times the hard-sphere rate constant provides markedly larger rate constants than those used by *Toumi* [1992]. Further, N_2 *v-v* transfer is included in the current study as well as that of O_2.

Figure 3 shows total N_2 and O_2 energy transfer rate constants used in this study. For N_2 (one-dot-dashed line) and O_2 (three-dots-dashed line), the total *v-v* transfer rate constant incorporating removal of one to five vibrational quanta from $O_2^\ddagger$ is shown, then the total quenching rate constant with both *v-v* and the *v-t* process (dashed line for N_2, solid line for O_2). The *v-t* contribution is a large fraction of the total energy transfer rate constant for O_2 collider gases for $O_2^\ddagger$ in *v* states greater than 15. For N_2 as a collider, *v-v* is a significant contributor to quenching only for *v* from 15 to 22 (compare the dashed line with the one-dot-dashed line). Further evaluation of the sensitivity of the $O_2^\ddagger$ processes to the choice of energy transfer rate constants is needed. Since the preliminary *v-t* quenching rate constants are markedly higher than those of *Toumi* [1992], which were based on previous experimental data of *Parker and Ritke* [1973], the contribution of each quenching process and collider to the $O_2^\ddagger$ effect should be established separately.

Four cases of the LLNL two-dimensional model are conducted including different sets of $O_2^\ddagger$ collisional quenching processes, as listed in Table 2. Case 1 includes only *v-v* transfer from $O_2^\ddagger$ by O_2, which is similar to the quenching used by *Toumi et al.* [1991]. Both N_2 and O_2 *v-v* transfer from $O_2^\ddagger$ are considered for case 2 in order to demonstrate the effect of the additional collider gas. The effect of the higher *v-v* transfer rate constants used here is demonstrated by case 3, including O_2 removal of $O_2^\ddagger$ by both *v-t* and *v-v* processes. Case 4 incorporates both *v-t* and *v-v* transfer by both N_2 and O_2, which is the situation in the real atmosphere.

$O_2^\ddagger$, once created by O_3 photolysis, may be either deactivated by collisional energy transfer as in equation (3) or photolyzed in the Schumann-Runge transition region by equation (2). The lifetime of $O_2^\ddagger$ is less than 1 hour, so that the instantaneous equilibrium or steady state approximation is applied to each of the species $O_2^\ddagger(v)$. The concentrations are then given by

$$\left[O_2^\ddagger(v)\right] = \frac{j_{O_3}(v)\left[O_3\right] + \sum_{M}\sum_{\Delta=1}^{5} k^{M}_{v,v+\Delta}[M]\left[O_2^\ddagger(v+\Delta)\right]}{j_{O_2^\ddagger(v)} + \sum_{M}\sum_{\Delta=1}^{5} k^{M}_{v-\Delta,v}[M]} , \qquad (11)$$

where the photolysis rate constants correspond to integrals over wavelength of the transition cross section, the solar flux, and the photolysis quantum yield. Note that $O_2^\ddagger$ may not be produced with *v* greater than its dissociation limit of 38.

TABLE 2. $O_2^\ddagger$ Quenching Cases Employed in the LLNL Two-Dimensional Model

M	N_2		O_2	
	v-v	*v-t*	*v-v*	*v-t*
case 1	no	no	yes	no
case 2	yes	no	yes	no
case 3	no	no	yes	yes
case 4	yes	yes	yes	yes

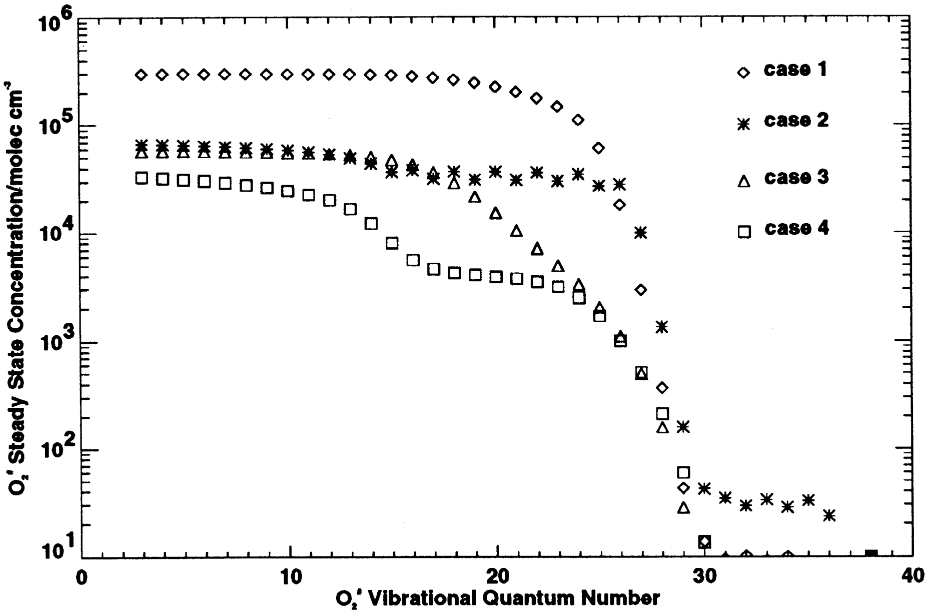

Fig. 4. Steady state concentrations of vibrationally excited oxygen versus vibrational quantum number for 30°N, 44 km at model autumn equinox. Diamonds case 1 (see Table 2); asterisks, case 2; triangles, case 3; squares, case 4.

MODEL-DERIVED $O_2^\ddagger$ AND O_3 CONCENTRATIONS AND KINETICS

For each of the four rate constant cases in Table 2, the LLNL two-dimensional model is integrated under present atmosphere conditions until a steady state is reached with respect to annual periodicity of ozone concentrations. Figure 4 illustrates steady state $O_2^\ddagger$ concentrations at noon on the autumn equinox with respect to vibrational quantum number. In case 1, the concentration of $O_2^\ddagger$ remains nearly constant at 3×10^5 molecules cm^{-3} up to $v = 20$, and falls off rapidly for higher v (diamonds). Inclusion of v-v transfer from N_2 (case 2) causes a loss in $O_2^\ddagger$ concentration of a factor about 5 for all v less than 25. When the v-v and v-t transfer of O_2 is considered (case 3), however, the decrease in $O_2^\ddagger$ concentrations is a factor of up to 20 for v from 15 to 22. Use of both N_2 and O_2 v-v and v-t transfer (case 4) produces $O_2^\ddagger$ concentrations slightly smaller than the O_2 v-v and v-t case at high v and slightly larger at low v: 3×10^4 molecules cm^{-3} for $v = 3$, decreasing throughout the range of v to 2×10^3 molecules cm^{-3} at $v = 25$. The additional quenching of the v-t transfer mode is particularly important in reducing the $O_2^\ddagger$ effect on odd oxygen compared with the calculation of *Toumi et al.* [1991]. *Toumi* [1992] used a v-t rate constant fit which yields considerably slower quenching than is found in the current study. The *Toumi* [1992] study provides steady state concentrations of $O_2^\ddagger$ for v from 15–24 at a solar zenith angle of 35 °N, corresponding to a latitude of 30°N in September, and a pressure of 0.72 mbar corresponding to 51 km altitude. These values are converted to concentration and compared with those found by our model at 30°N, 0.690 mbar (52.5 km) in Table 3. Our case 4 produces $O_2^\ddagger$ concentrations considerably smaller than those of either Toumi case.

The rate of O atom production from $O_2^\ddagger$ also depends upon the rate of O_3 photolysis, the solar flux, and the absorption cross section of $O_2^\ddagger$. For the four cases, the rate of $O_2^\ddagger$ photolysis in molecules cm^{-3} s^{-1} (one half of the O atom production rate) at 30°N, autumn equinox noon is plotted against v in Figure 5. The $O_2^\ddagger$ photolysis rate peaks at 1×10^4 molecules cm^{-3} s^{-1} about $v = 20$ with O_2 v-v quenching only (case 1), with considerable contributions for v down to 12 and up to 24. In case 2, the photolysis rate decreases by a factor of nearly 10 throughout that v range because N_2 v-v removal of two $O_2^\ddagger$ quanta coincides well with the peak of odd oxygen production for case 1 (see Figure 3). Inclusion of both v-v and v-t quenching for O_2 also produces a factor of nearly 10 decline in photolysis rates, which also pushes the production to lower v as the high v $O_2^\ddagger$ are quenched faster (case 3). Addition of N_2

TABLE 3. Steady State $O_2^\ddagger$ Concentrations (10^4 molecules cm^{-3}) in the LLNL Two-Dimensional Model at 30°N, 52.5 km Compared With *Toumi* [1992]

	This Work				Toumi (1992)	
v	Case 1	Case 2	Case 3	Case 4	Case A	Case B
15	25.07	2.44	4.67	0.644	7.9	17.7
16	24.73	2.49	4.39	0.497	7.9	19.7
17	24.13	2.16	3.95	0.430	7.9	21.6
18	23.15	2.40	3.32	0.396	7.9	21.6
19	21.63	2.10	2.57	0.380	5.9	19.7
20	19.54	2.36	1.81	0.361	5.9	17.7
21	16.90	2.06	1.17	0.344	3.9	15.7
22	13.91	2.31	0.716	0.308	3.9	11.8
23	10.90	1.97	0.441	0.262	2.0	7.9
24	7.55	2.17	0.263	0.192	2.0	5.9

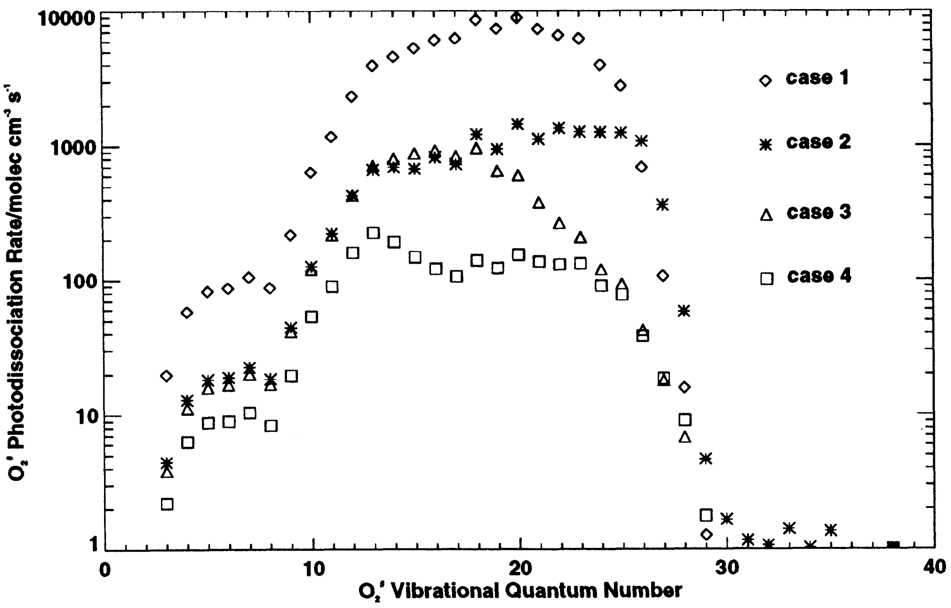

Fig. 5. Rates of photolysis for vibrationally excited oxygen plotted against vibrational quantum number for 30°N, 44 km at model autumn equinox. Diamonds, case 1 (see Table 2); asterisks, case 2; triangles, case 3; squares, case 4.

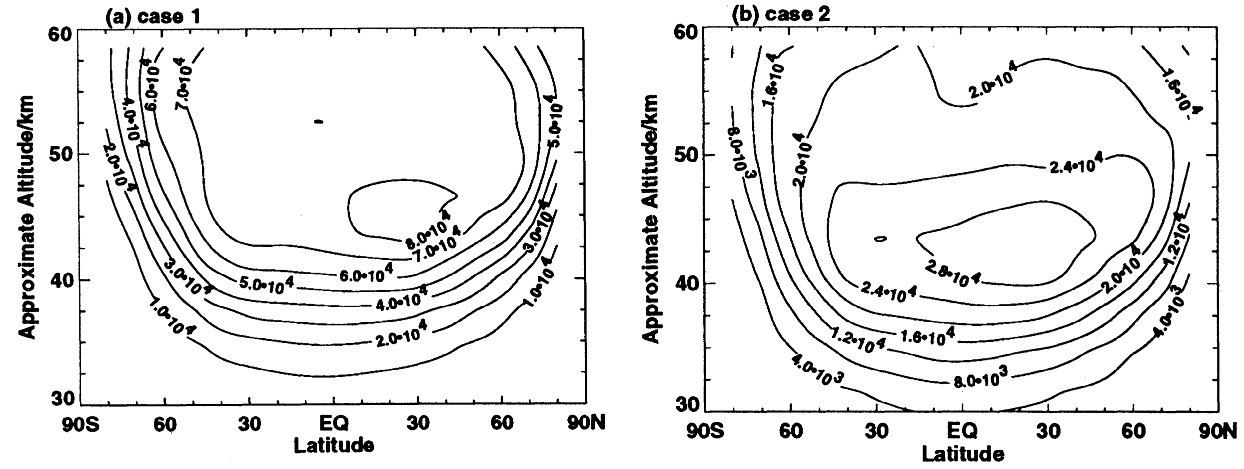

(a) case 1

(b) case 2

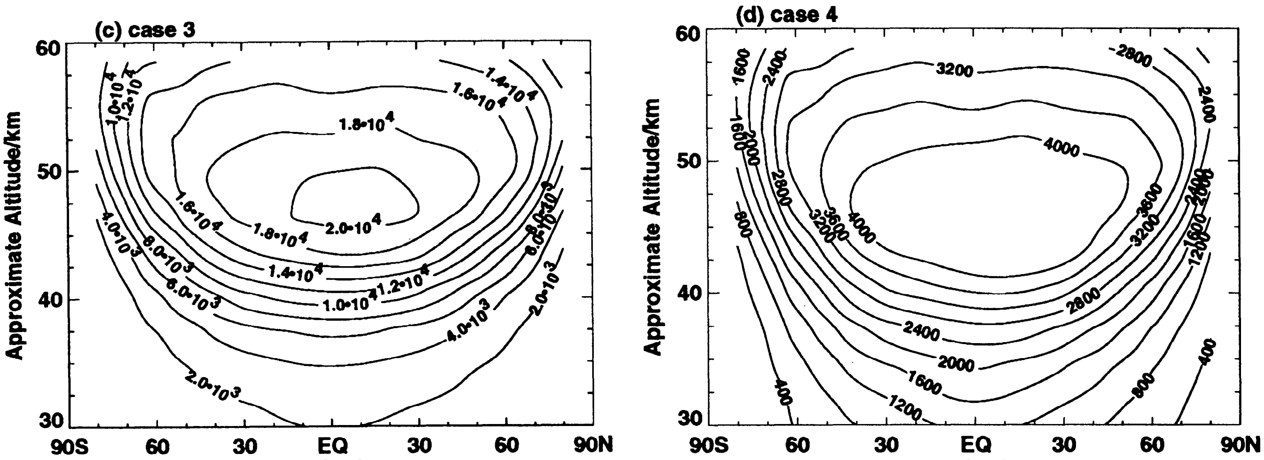

(c) case 3

(d) case 4

Fig. 6. Oxygen atom production rates (atoms cm^{-3} s^{-1}) from vibrationally excited oxygen in the LLNL two-dimensional model at autumn equinox for (*a*) case 1, (*b*) case 2, (*c*) case 3, and (*d*) case 4.

v-v and v-t quenching to that case produces another factor of 10 decrease in the photolysis rate (case 4); the maximum contribution becomes 200 molecules cm^{-3} s^{-1} at $v = 12$, and the photolysis rate falls off with v to either direction. The strongest contribution to O atom production from $O_2^‡$ comes from v in the range of 10 to 25, and the higher v are most severely affected by use of the full quenching model both in terms of concentration and in terms of photolysis rate. Figure 6 illustrates the O atom production rate from $O_2^‡$, (total over v) at noon on the autumn equinox as a function of latitude and altitude. Altitudes less than 30 km are omitted in Figures 6*a*–6*d* and the next due to the decreasing importance of molecular oxygen dissociation to ozone production at those altitudes. In all four cases, the rate peaks somewhat north of the Equator at altitudes from 43 to 50 km. However, the maximum value for case 1 (Figure 6*a*) is 8.4×10^4 molecules cm^{-3} s^{-1}, that for case 2 (Figure 6*b*) is 1.6×10^3 molecules cm^{-3} s^{-1}, that for case 3 (Figure 6*c*) is 1.1×10^4 molecules cm^{-3} s^{-1}, and that for case 4 (Figure 6*d*) is 2.4×10^3 molecules cm^{-3} s^{-1}. Figure 7 illustrates the ratio of the $O_2^‡$ dissociation rate to the thermal O_2 dissociation rate at the autumn equinox for the four cases. The $O_2^‡$ process adds up to 4.2% to the odd oxygen production rate in case 1 (Figure 7*a*) located at the top of the model atmosphere, 50 °N. Adding N_2 v-v for case 2 decreases the odd oxygen enhancement to a maximum of 0.5%. The upper atmosphere odd oxygen enhancement in case 3 (Figure 7*c*) shows a slightly further decrease, to a maximum of 0.4%. Finally, the most realistic case 4 reduces the ratio to a maximum of 0.1% (Figure 7*d*).

The O_3 concentration is expected to increase by nearly the same percentage as does the O atom production from $O_2^‡$ processes in the upper stratosphere. Figure 8*a* demonstrates the percentage increase in O_3 concentration for case 1 on December 21 as compared with an ambient atmosphere in the absence of $O_2^‡$ processes. The 4.0% maximum increase in ozone is markedly less than the results of *Toumi et al.* [1991]. Figure 8*b* shows the enhancement for case 2; the greatest enhancement is 0.49% at the top of the model atmosphere for northern latitudes. In Figure 8*c*, representing case 3, the maximum upper atmosphere ozone enhancement of 0.33% occurs at the top of the model atmosphere about 50°N. When case 4 with v-v and v-t and with N_2 and O_2 is invoked, as shown in Figure 8*d*, the ozone enhancement from $O_2^‡$ is reduced still further to 0.27%. Figures 8*b*–*d* also indicate slight calculated enhancements in ozone of 0.5% in the upper troposphere and the equatorial tropopause; these, however, are only slight increases occurring at the minimum of atmospheric ozone concentration.

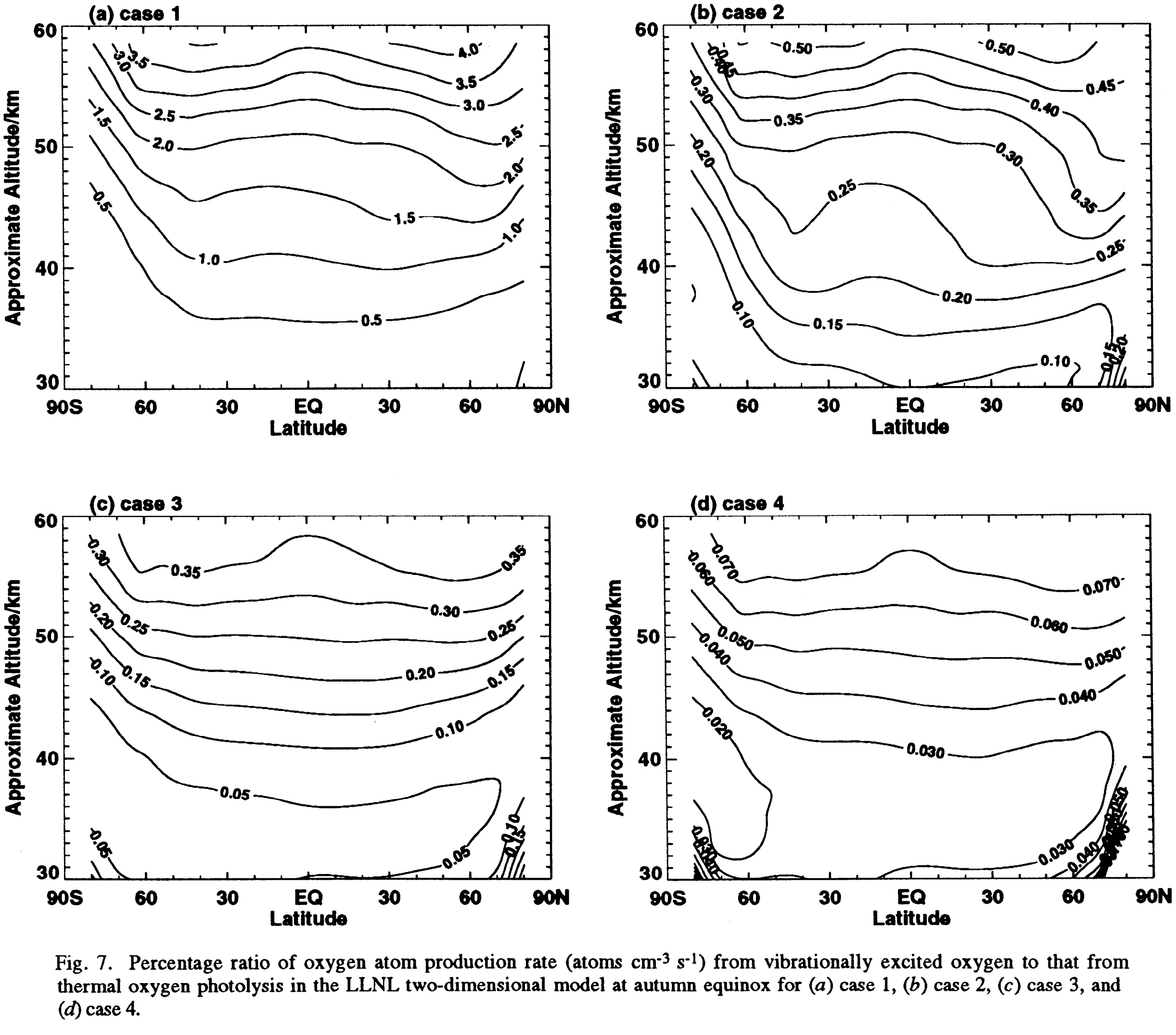

Fig. 7. Percentage ratio of oxygen atom production rate (atoms cm^{-3} s^{-1}) from vibrationally excited oxygen to that from thermal oxygen photolysis in the LLNL two-dimensional model at autumn equinox for (*a*) case 1, (*b*) case 2, (*c*) case 3, and (*d*) case 4.

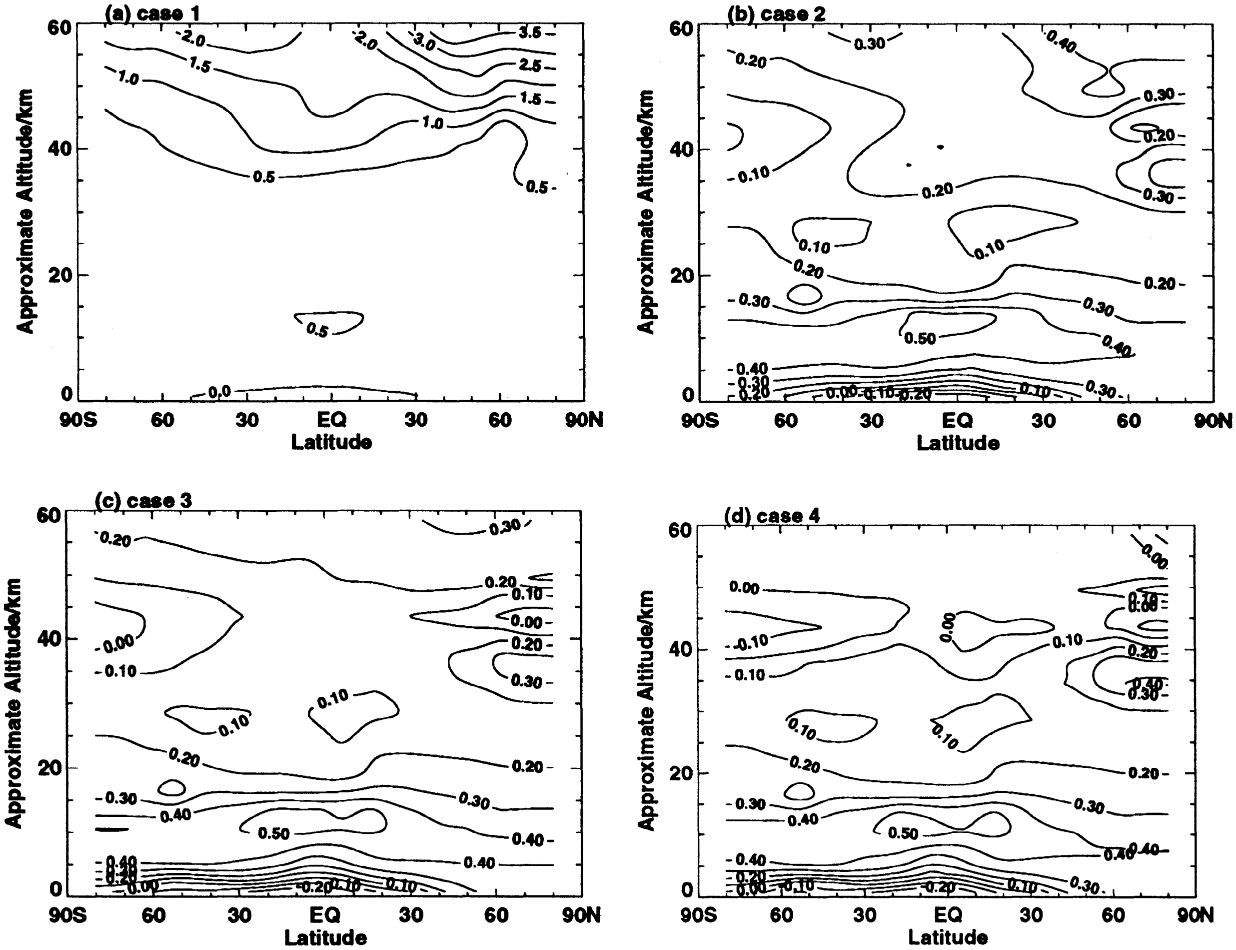

Fig. 8. Ozone concentration increase (percent) in the LLNL two-dimensional model with $O_2^\ddagger$ processes compared with ambient atmosphere without $O_2^\ddagger$ at winter solstice for (*a*) case 1, (*b*) case 2, (*c*) case 3, and (*d*) case 4.

An estimate of the extent to which the $O_2^\ddagger$ ozone enhancement does not satisfy the ozone deficit is given by Figure 9. Model O_3 concentrations on the autumn equinox at 30°N are plotted against altitude, along with results from UARS MLS and published climatological zonal mean values [*Keating et al.*, 1989]. Even for case 1 (diamonds), the O_3 concentration is only slightly greater for all altitudes above 32 km. The resulting concentrations remain lower than the uncertainty limits of the measurements of the UARS MLS (asterisks with error bars) and the climatological values for September at 30°N (crosses) for log-pressure altitudes between 32 and 50 km. MLS data are seen to agree well with the climatological values from *Keating et al.* [1989]. The MLS measurements are an average of data taken from 28°N to 32°N latitude for September 21, 1991 for the 205 GHz O_3 band. The error bars represent the actual rms deviations about the mean values. Absolute accuracy of MLS data is still under investigation, but intercomparisons of MLS ozone (from the 205 GHz band) with other data sets produce no concern about the accuracy of the plotted values for the altitudes shown here. The change in ozone profile between the LLNL two-dimensional model without $O_2^\ddagger$ processes (triangles) and the most realistic case examined, case 4, incorporating both v-v and v-t processes with both N_2 and O_2 as colliders (squares), is insignificant on the scale of Figure 9.

Inclusion of *v-t* energy transfer processes and of N_2 as a collider have been shown to reduce the potential for ozone enhancement produced by $O_2^\ddagger$ processes in the model upper atmosphere. Since the quenching rate constants used here are preliminary, one concern is the extent to which the current choice of rate constants limits the calculated ozone enhancement. That is, how small should quenching rate constants be in order for models of the atmosphere to consider $O_2^\ddagger$ processes? We explore this question in a further series of model cases reported below.

The LLNL two-dimensional chemical-radiative-transport model with $O_2^\ddagger$ processes is again integrated to steady state in these cases. The individual energy transfer rate constants for these cases are set to a specified fraction, ranging from 0.001 to 0.1, of those used for case 4, the N_2 and O_2, *v-v* and *v-t* quenching case. The resulting December 21 ozone concentration at 30°N, 49.5 km is then compared with that in the ambient atmosphere at the same latitude and altitude to find the ozone enhancement. Figure 10 shows the ozone enhancement as a function of the fraction of the case 4 quenching rate constants used. The log-log plot shows that this function closely follows a reciprocal function. Note that equation (11) in the limit where the photolysis rate constant of $O_2^\ddagger$ is insignificant compared to the quenching rate constant

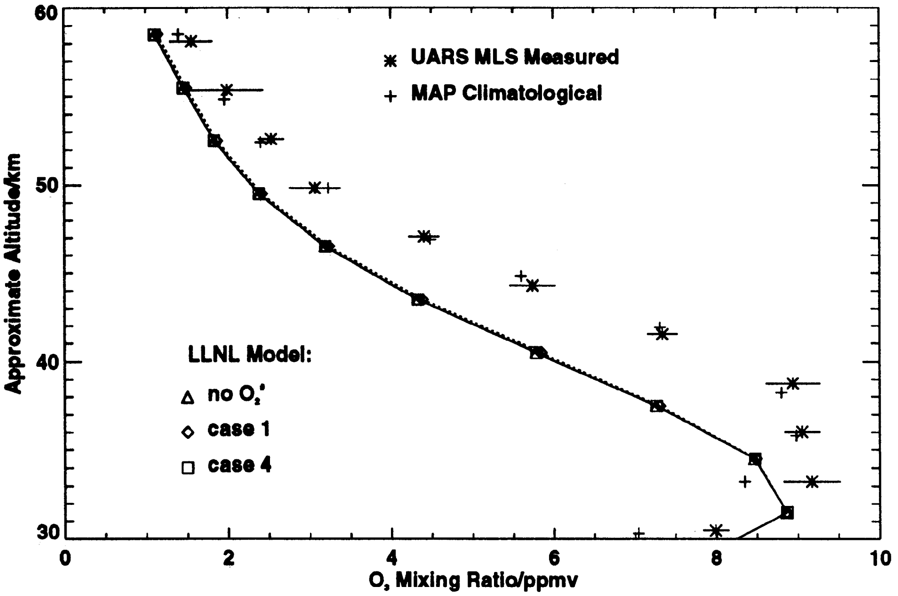

Fig. 9. Comparison of Upper Atmosphere Research Satellite Microwave Limb Sounder (UARS MLS) measurements of ozone concentration with the LLNL two-dimensional model at autumn equinox, 30°N. Asterisks, UARS MLS (lines represent one standard deviation about the mean from 28 to 32°N); crosses, Middle Atmospheric Program (MAP) recommended values (10-% typical uncertainty); triangles, LLNL two-dimensional ambient atmosphere (no $O_2^‡$); diamonds, LLNL two-dimensional model, O_2 v-v quenching (case 1); squares, LLNL two-dimensional model, full quenching model (case 4).

would leave a reciprocal-like dependence on k_c, the sum of $k^M_{v-\Delta,v}$. Quenching rate constants some 0.05 times the full quenching case are sufficient to ozone enhancement of 1%. By comparison, the comparison of ozone concentrations between models and measurements in *WMO* [1985 Section 8] indicates a deficit ranging from 13% to 60%, though the averaged measurements are considered uncertain (2σ) to some 10%. *Eluszkiewicz and Allen* [1993] compared ozone from a photochemical model with temperature, water vapor, and NO_2 based on measurements by LIMS and with ClO determined by a separate calculation with LIMS ozone measurements. Their simulation of May 1–7, 1979, produces some 10% lower ozone at 49.5 km, 30°N than is measured. In the LLNL model, enhancements of 10% could be produced only if the quenching constants were some 1/200 of those used in case 4. Though the rate constants defined above as the full quenching case are

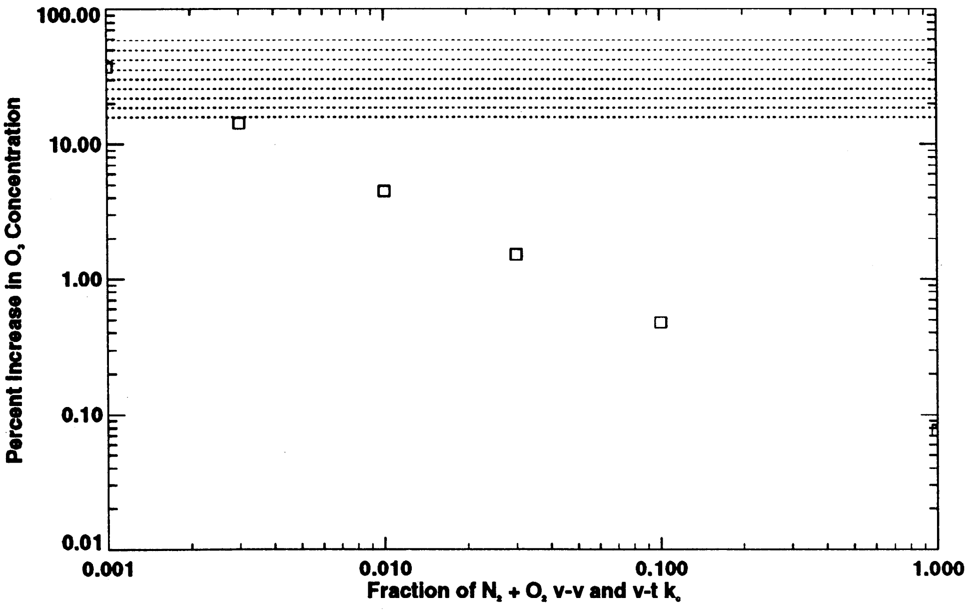

Fig. 10. Percentage enhancement in ozone concentration at 30°N, 49.5 km log-pressure altitude (1.047 mbar) is plotted as squares for the LLNL two-dimensional model with $O_2^‡$ processes against collisional energy transfer rate constant. These rate constants are those of the full quenching model of case 4 multiplied by factors ranging from 0.001 to 1.0. The dotted area indicates the ozone deficit range found in Figure 8-8 of World Meteorological Organization [1985] for that latitude and altitude.

subject to change, this analysis shows that the $O_2^{\ddagger}$ process is unlikely to account for the full upperstratospheric ozone deficit in current atmospheric models.

CONCLUSIONS

Odd oxygen production from the photolysis of vibrationally excited oxygen $O_2^{\ddagger}$ produced by ultraviolet photolysis of ozone (O_3) in the upper stratosphere has been incorporated in the LLNL two-dimensional global stratosphere-troposphere model. When quenching of $O_2^{\ddagger}$ only by v-v collisional energy transfer to O_2 is considered, odd oxygen production rates throughout the upper stratosphere (>30 km) increase by up to 4.0%, with a corresponding increase in O_3 concentration. This ozone enhancement is markedly smaller than that of *Toumi et al.* [1991], but agrees qualitatively with *Toumi* [1992]. However, when we extend this study by including a determined rate for v-t collisional energy transfer and including N_2 as a collider gas, the odd oxygen contribution from $O_2^{\ddagger}$ processes is greatly reduced. These effects on ozone are insignificant compared with thermal O_2 photolysis. The sensitivity of $O_2^{\ddagger}$ processes in the stratosphere to detailed energy transfer rate constants is well demonstrated here; unfortunately, these constants are not yet well determined in the laboratory. While the detailed input parameters of $O_2^{\ddagger}$ are not currently available from experiment, use of preliminary quenching rate constants indicates that $O_2^{\ddagger}$ processes are not sufficient to explain the systematic underestimation of upper stratospheric O_3 concentrations in models of stratospheric chemistry.

Acknowledgments. This work was performed under the auspices of the U.S. Department of Energy by the Lawrence Livermore National Laboratory under contract W-7405-Eng-48 and was supported in part by the U.S. Department of Energy (DOE) Office of Health and Environmental Research's Environmental Sciences Division and by the National Aeronautics and Space Administration Upper Atmosphere Research Satellite program. K.P. also appreciates appointment to the Global Change Distinguished Postdoctoral Fellowships sponsored in part by the U.S. DOE, Office of Health and Environmental Research, and administered by Oak Ridge Associated Universities. We thank J. Waters of the Jet Propulsion Laboratory for discussions related to the ozone data from the Upper Atmosphere Research Satellite, D. L. Huestis and R. P. Saxon at SRI International for many helpful discussions concerning this study, and K. Kulander and B. P. Lengsfield of LLNL for use of and guidance in their vibrational wavefunction code.

REFERENCES

Allen, M., and J. E. Frederick, Effective photodissociation cross sections for molecular oxygen and nitric oxide in the Schumann-Runge bands, *J. Atmos. Sci.*, *39*, 2066–2075, 1982.

Allison, A. C., A. Dalgarno, and N. W. Pasachoff, Absorption by vibrationally excited molecular oxygen in the Schumann-Runge continuum, *Planet. Space Sci.*, *19*, 1463–1473, 1971.

Allison, A. C., S. L. Guberman, and A. Dalgarno, A model of the Schumann-Runge continuum of O_2, *J. Geophys. Res.*, *91*, 10,193–10,198, 1986.

Barnett, J. J., and M. Corney, Middle atmosphere reference model derived from satellite data, in *Middle Atmosphere Program: Handbook for MAP*, *18*, SCOSTEP Secretariat, University of Illinois, Urbana, Ill., pp. 47–86, 1985.

Butler, D. M., The uncertainty in ozone calculations by a stratospheric photochemistry model, *Geophys. Res. Lett.*, *5*, 769–772, 1978.

Cheung, A. S.-C., K. Yoshino, W. H. Parkinson, and D. E. Freeman, Molecular spectroscopic constants of $O_2(B^3S^-{}_u)$: The upper state of the Schumann-Runge bands, *J. Mol. Spectrosc.*, *119*, 1–10, 1986.

Creek, D. M., and R. W. Nicholls, A comprehensive re-analysis of the $O_2(B\ {}^3S_u^-\ \text{-}\ X\ {}^3S_g^-)$ Schumann-Runge band system, *Proc. R. Soc. London*, Ser. *A*, *341*, 517–536, 1975.

DeMore, W. B., S. P. Sander, R. F. Hampson, M. J. Kurylo, D. M. Golden, C. J. Howard, A. R. Ravishankara, and M. J. Molina, *Chemical Kinetics and Photochemical Data for Use in Stratospheric Modeling: Evaluation Number 9*, Jet Propulsion Laboratory, California Institute of Technology, Pasadena, California, 1990.

Eluszkiewicz, J., and M. Allen, A global analysis of the ozone deficit in the upper stratosphere and lower mesosphere, *J. Geophys. Res.*, *98*, 1069–1082, 1993.

Fleming, E. L., S. Chandra, M. R. Schoeberl, and J. J. Barnett, Monthly mean global climatology of temperature, wind geopotential height, and pressure for 0–120 km, *NASA Tech. Memo.*, *1000697*, 1988.

Garcia, R. R., and S. Solomon, A numerical model of the zonally averaged dynamical and chemical structure of the middle atmosphere, *J. Geophys. Res.*, *88*, 1379–1400, 1983.

Harshvardhan, R. Davies, D. A. Randall, and T. G. Corset, A fast radiation parameterization for atmospheric circulation models, *J. Geophys. Res.*, *92*, 1009–1016, 1987.

Johnston, H. S., D. E. Kinnison, and D. J. Wuebbles, Nitrogen oxides from high-altitude aircraft: an update of potential effects on ozone, *J. Geophys. Res.*, *94*, 16,351–16,363, 1989.

Keating, G. M., M. C. Pitts, and D. F. Young, Ozone reference models for the middle atmosphere (New CIRA), in *Middle Atmosphere Program: Handbook for MAP*, *31*, pp. 1–36, SCOSTEP Secretariat, University of Illinois, Urbana, Ill., 1989.

Kinugawa, T., T. Sato, T. Arikawa, Y. Matsumi, and M. Kawasaki, M., Formation of $O(^3P_j)$ photofragments from the Hartley band photodissociation of ozone at 226 nm, *J. Chem. Phys.*, *93*, 3289–3294, 1990.

Krupenie, P. H., The spectrum of molecular oxygen, *J. Phys. Chem. Ref. Data*, *1*, 423–534, 1972.

Kulander, K. C., Spectroscopy of SO, *Chem. Phys. Lett.*, *149*, 392–396, 1988.

Laher, R. R., and F. R. Gilmore, Improved fits for the vibrational and rotational constants of many states of nitrogen and oxygen, *J. Phys. Chem. Ref. Data*, *20*, 685–712, 1991.

Levine, I. N., *Molecular Spectroscopy*, pp. 306–308, John Wiley, New York, 1975.

Lewis, B. R., L. Berzins, and J. H. Carver, Oscillator strengths for the Schumann-Runge bands of $^{16}O_2$, *J. Quant. Spectrosc. Radiat. Transfer*, *36*, 209–232, 1986.

Newman, P. A., M. R. Schoeberl, R. A. Plumb, and J. Rosenfield, Mixing rates calculated from potential vorticity, *J. Geophys. Res.*, *93*, 5221–5240, 1988.

Oort, A. H., Global atmospheric circulation statistics, 1958–1973, *NOAA Prof. Pap. 14*, U.S. Dept. of Commer., Natl. Oceanic and Atmos. Admin., Washington, D. C., April 1983.

Park, H., and T. G. Slanger, $O_2(X)$ vibrational distribution from O_3 photodissociation at 248 nm, *J. Chem Phys.*, in press, 1994.

Parker, J. G., and D. N. Ritke, Vibrational relaxation times of oxygen in the pressure range 10–110 atm, *J. Chem. Phys.*, *58*, 314–323, 1973.

Patten, K. O., Jr., P. S. Connell, D. E. Kinnison, D. J. Wuebbles, J. Waters, L. Froidevaux, and T. G. Slanger, An investigation of the processes controlling ozone in the upper stratosphere, *Proceedings of the International Quadrennial Ozone Symposium 1992*, in press.

Rapp, D., Interchange of vibrational energy between molecules in collisions, *J. Chem. Phys.*, *43*, 316–317, 1965.

Rapp, D., and P. Englander-Golden, Resonant and near-resonant vibrational-vibrational energy transfer between molecules in collisions, *J. Chem. Phys.*, *40*, 573–575, 1964.

Rapp, D., and T. E. Sharp, Vibrational energy transfer in molecular collisions involving large transition probabilities, *J. Chem. Phys.*, *38*, 2641–2648, 1963.

Saxon, R. P., and T. G. Slanger, Relative contributions of discrete and continuum absorption to the photodissociation of vibrationally excited O_2 (v = 12–20), *J. Geophys. Res.*, *96*, 17,291–17,295, 1991.

Slanger, T. G., L. E. Jusinski, G. Black, and G. E. Gadd, A new laboratory source of ozone and its potential atmospheric implications, *Science*, *241*, 945–950, 1988.

Smolarkiewicz, P. K., A fully multidimensional positive definitive advection transport algorithm with small implicit diffusion, *J. Comput. Phys.*, *54*, 325–362, 1984.

Toumi, R., An evaluation of autocatalytic ozone production from vibrationally excited oxygen in the middle atmosphere, *J. Atmos. Chem.*, *15*, 69–77, 1992.

Toumi, R., B. J. Kerridge, and J. A. Pyle, Highly vibrationally excited oxygen as a potential source of ozone in the upper stratosphere and mesosphere, *Nature*, *351*, 217–219, 1991.

Truhlar, D. G., Finite difference boundary value method for solving one-dimensional eigenvalue equations, *J. Comput. Phys.*, *10*, 123–132, 1972.

Vaghjiani, G. L., and A. R. Ravishankara, New measurement of the rate coefficient for the reaction of OH with methane, *Nature*, *350*, 406–409, 1991.

Valentini, J. J., D. P. Gerrity, D. L. Phillips, J.-C. Nieh, and K. D. Tabor, CARS spectroscopy of $O_2(^1\Delta_g)$ from the Hartley band photodissociation of O_3: Dynamics of the dissociation, *J. Chem. Phys.*, *86*, 6745–6756, 1987.

Wolfram, S., *Mathematica: a System for Doing Mathematics by Computer*, Addison-Wesley, Reading, Mass., 1988.

World Meteorological Organization, Atmospheric ozone 1985: Assessment of our understanding of the processes controlling its present distribution and change, Rep. 16, Geneva, 1985.

World Meteorological Organization, Scientific assessment of ozone depletion, Rep. 25, United Nations Environment Programme Global Ozone Res. and Monitoring Project, Geneva, 1991.

Wuebbles, D. J., D. E. Kinnison, K.E. Grant, and J. Lean, The effect of solar flux variations and trace gas emissions on recent trends in stratospheric ozone and temperature, *J. Geomagn. Geoelectr.*, *43*, suppl., 709-718, 1991.

Yardley, J. T., *Introduction to Molecular Energy Transfer*, Academic, San Diego, Calif., 1980.

P.S. Connell, D.E. Kinnison, K.O. Patten, and D.J. Wuebbles, Lawrence Livermore National Laboratory, L-262, P.O. Box 808, Livermore, CA 94550.
L. Froidevaux, Jet Propulsion Laboratory, Pasadena, CA 91109
T.G. Slanger, SRI International, Menlo Park, CA 94025

(Received January 26, 1993;
revised August 27, 1993;
accepted September 7, 1993.)